

# Effect of Small-Scale Output Unsteadiness on Adjoint-Based Sensitivity

Joshua A. Krakos\* and David L. Darmofal†

Massachusetts Institute of Technology, Cambridge, Massachusetts 02139

DOI: 10.2514/1.J050412

**This paper investigates the impact of small-scale unsteadiness on adjoint-based output sensitivity analysis. In particular, when iterative methods for nonlinear flows fail to converge to a steady state, it is demonstrated that the resulting sensitivity analysis can be highly inaccurate, even when the unsteadiness in the outputs is small. The specific example considered is the viscous subsonic flow around an airfoil over a range of angles of attack. If a strengthened solver is used to solve the adjoint equation (even though the flow equations did not fully converge), it is demonstrated that the sensitivity of the lift with respect to angle of attack can vary significantly, due to linearizing about different solution iterates of the steady flow solver. Further, the unsteady iterates from the time-inaccurate steady-state solver to the time-accurate solution are compared. The unsteadiness of the time-accurate solution is markedly different from the iterate solutions of the steady-state solver. If a strengthened solver is applied to the nonlinear flow equations, steady solutions can be achieved whose lift is significantly different from the time-averaged lift of the time-accurate simulations. Time-accurate unsteady adjoint analysis is then shown to provide accurate sensitivities for the time-averaged lift.**

## Nomenclature

$A, B$	=	dummy matrices
$C_L$	=	lift coefficient
$f$	=	nonlinear system of equations
$\tilde{f}_e$	=	semidiscrete unsteady nonlinear system of equations
$g$	=	output function
$i$	=	time-step index
$\mathcal{J}, J$	=	continuous/discrete output functional of interest
$\mathcal{L}, L$	=	continuous/discrete system Lagrangian
$\mathcal{M}$	=	finite element mass matrix
$M_P$	=	preconditioning matrix approximation to system Jacobian inverse
$Ma$	=	Mach number
$m$	=	number of equations in system of equations
$N$	=	number of time steps across time span of interest
$p$	=	polynomial order of solution
$R$	=	partial differential equation weak residual
$\mathbb{R}$	=	the set of real numbers
$Re$	=	Reynolds number
$t$	=	time
$t_f$	=	final time
$U$	=	partial differential equation primal solution vector
$u$	=	primal solution state
$v, w$	=	dummy variable for primal/dual state
$\alpha$	=	angle of attack
$\beta$	=	control parameter
$\Delta t$	=	time step
$\delta$	=	variation of a function or variable
$\lambda$	=	right eigenvalue of a matrix

$\Psi$	=	partial differential equation dual (adjoint) solution vector
$\psi$	=	dual (adjoint) solution vector

## Subscripts

$e$	=	unsteady (time-dependent) variable or functional
$H$	=	discontinuous Galerkin discrete vector/functional on grid with characteristic length $H$
$i$	=	variable at time step/iteration $i$
$ss$	=	steady-state variable

## Superscript

0	=	initial condition
---	---	-------------------

## I. Introduction

WITH its roots in the calculus of variations, adjoint analysis has long been used in optimal control theory (as a reference, see Bryson and Ho [1]) and in weather model tuning [2–4]. Its use within the context of aerodynamics design is more recent and has been applied to design optimization [5–7] and to error estimation [8–13]. In aerodynamic design optimization, the sensitivity of an output with respect to design inputs is a key component in improving toward an optimal solution. In the case in which the number of inputs is large compared to the number of outputs, the adjoint can be computationally superior to other methods, providing a rigorous and efficient means of computing the required output parameter sensitivities. Furthermore, adjoint-based error estimation addresses the difficulty of determining, either by a priori or a posteriori means, regions of grid sensitivity for a given output and allows for automated and rigorous mesh refinement algorithms.

Because of the overall cost of unsteady analysis of both the primal and the adjoint, adjoint analysis in aerodynamics has been predominantly for steady problems. As the use of adjoint methods continues to increase within aerodynamics design, however, more problems are encountered for which a steady solution may not be appropriate or may not even exist: e.g., problems with regions of separation. For complex geometries and equation sets, the necessity of a steady-state solution places what may be an unrealistic robustness requirement on the primal flow solver [14].

Campobasso and Giles [15] investigated the effects of flow instabilities in the linear analysis of turbomachinery aeroelasticity. The authors found that the fixed-point iteration they used to solve the

Presented as Paper 2009-4274 at the 19th AIAA Computational Fluid Dynamics Conference, San Antonio, TX, 22–25 June 2009; received 13 January 2010; revision received 3 May 2010; accepted for publication 18 June 2010. Copyright © 2010 by Joshua A. Krakos and David L. Darmofal. Published by the American Institute of Aeronautics and Astronautics, Inc., with permission. Copies of this paper may be made for personal or internal use, on condition that the copier pay the \$10.00 per-copy fee to the Copyright Clearance Center, Inc., 222 Rosewood Drive, Danvers, MA 01923; include the code 0001-1452/10 and \$10.00 in correspondence with the CCC.

\*Doctoral Candidate, Aerospace Computational Design Laboratory, 77 Massachusetts Avenue, Room 37-401; Specialist Engineer, The Boeing Company, P.O. Box 516, St. Louis, MO 63166, Mail Code S306-4030. Member AIAA.

†Professor, Aerospace Computational Design Laboratory, 77 Massachusetts Avenue, Room 33-207. Associate Fellow AIAA.

linearized Navier–Stokes equations was not stable for cases in which the nonlinear background flow calculation did not converge to a steady solution but instead reached a small-amplitude limit cycle. While this unsteadiness in the primal nonlinear problem was small, the authors showed that the linearized system about a typical iterate of the unsteady solution had unstable eigenvalues. As a result, the iterative algorithm diverged when applied to the primal problem linearized about this state. These unstable modes are salient to the adjoint, because the eigenvalues of the adjoint problem are the same as those of the linearized primal problem for the same iterative solver [16]. Nemeć et al. [17] note a similar difficulty in an adjoint-based adaptive inviscid simulation of the flow about a complex launch abort vehicle. In their case, unsteadiness is encountered as the grid is adapted and wakes are refined. In the event of this small-scale unsteadiness, Campobasso and Giles [15] proposed stabilizing the iterative scheme for the linearized equations using GMRES [18] or the recursive projection method [19,20]. With this approach, the linearized equations can be solved and the sensitivity analysis can be performed about an unconverged iterate from the steady nonlinear primal solver.

Parameter sensitivities and error estimates based on the adjoint require that the primal problem be satisfied, and applying steady adjoint methods to unconverged solution iterates introduces an error contribution from that nonconvergence, even when the output is relatively unaffected. As a result, the parameter sensitivity or error estimate computed from the adjoint at an arbitrary state in an unconverged iterative solution method will be dependent on the particular state at which the adjoint is computed. The variability in the sensitivity due to linearization about unconverged iterates is demonstrated for the viscous subsonic flow about a NACA 0012 airfoil at a moderate angle of attack in Sec. IV.

Even if the nonlinear primal solver can be strengthened such that steady solutions can be achieved, a steady solution may be quite different from, say, the time average of an unsteady solution. As a result, although a steady sensitivity analysis may be possible, the resulting sensitivity may not be physically relevant (assuming that the unsteady solution is more likely to occur in practice). This difference between the steady and unsteady behavior is demonstrated for the airfoil example in Sec. V.

Rather than calculate a steady primal and adjoint solution, a time-dependent flow and adjoint analysis can be preformed. The unsteady adjoint has the benefit that the result is applicable for both small- and large-scale unsteady behavior. However, a straightforward implementation of the unsteady adjoint requires the storage of the entire primal solution for the time period of interest. This storage requirement has led to check-pointing methods [21], trading some of the solution storage overhead for additional recomputation but without fundamentally changing the underlying algorithm. Despite its cost, the unsteady adjoint has received increased interest by the computational fluid dynamics community in the last decade. Nadarajah and Jameson [22] focus on aerodynamics shape optimization in the context of finite volume formulations. Mani and Mavriplis [23] and Mavriplis [24] investigated an unsteady discrete adjoint formulation for output matching and minimization applied to two- and three-dimensional flow problems. Additionally, Rumpfkeil and Zingg [25] applied the discrete adjoint to aeroacoustic shape design.

The remainder of this paper is organized as follows. Adjoint methods are reviewed for stationary and time-dependent primal solutions in Sec. II. Then a model problem that exhibits small-scale output unsteadiness when attempting to solve a single-point flow solution will be introduced in Sec. III. In Sec. IV, the use of steady adjoint analysis is investigated for the stationary-point solution of the model problem and solutions from (unconverged) arbitrary iterations. Finally, in Sec. V, we apply unsteady adjoint analysis to the time-accurate flow simulations.

## II. Adjoint Formulation

In this section, adjoint analysis for output parameter sensitivities is reviewed for steady and time-dependent problems. Iterative techniques used to solve the resulting adjoint equations are also described.

### A. Steady Adjoint

To develop the adjoint formulation, first introduce the steady nonlinear system for the primal problem:

$$\mathbf{f}(\mathbf{u}_{ss}; \beta) = \mathbf{0} \quad (1)$$

where  $\mathbf{f}(\mathbf{u}_{ss}; \beta): \mathbb{R}^m \times \mathbb{R} \rightarrow \mathbb{R}^m$  is a nonlinear residual statement,  $\mathbf{u}_{ss} \in \mathbb{R}^m$  is the primal state vector with  $m$  components, and  $\beta \in \mathbb{R}$  is an input parameter. Let  $\mathcal{J}(\beta) = g(\mathbf{u}_{ss}; \beta): \mathbb{R}^m \times \mathbb{R} \rightarrow \mathbb{R}$  be a general nonlinear functional output of interest. The Lagrangian is then defined as  $\mathcal{L}(\mathbf{v}, \mathbf{w}; \beta): \mathbb{R}^m \times \mathbb{R}^m \times \mathbb{R} \rightarrow \mathbb{R}$ :

$$\begin{aligned} \mathcal{L}(\mathbf{v}, \mathbf{w}; \beta) &\equiv g(\mathbf{v}; \beta) - \mathbf{w}^T \mathbf{f}(\mathbf{v}; \beta) \\ \forall \mathbf{v}, \mathbf{w} \in \mathbb{R}^m \quad \text{and} \quad \beta \in \mathbb{R} \end{aligned} \quad (2)$$

that is, the nonlinear system is adjoined to the output functional via an adjoint, or dual, state. Taking the first variation of  $\mathcal{L}$  with respect to  $\mathbf{v}$ ,  $\mathbf{w}$ , and  $\beta$ ,

$$\begin{aligned} \delta \mathcal{L}(\mathbf{v}, \mathbf{w}; \beta; \delta \mathbf{v}, \delta \mathbf{w}; \delta \beta) &= \delta \mathbf{v}^T [g_{\mathbf{v}}^T(\mathbf{v}; \beta) - \mathbf{w}^T \mathbf{f}_{\mathbf{v}}(\mathbf{v}; \beta)] \\ &\quad - \delta \mathbf{w}^T [\mathbf{f}(\mathbf{v}; \beta)] + \delta \beta [g_{\beta}^T(\mathbf{v}; \beta) - \mathbf{w}^T \mathbf{f}_{\beta}(\mathbf{v}; \beta)] \end{aligned} \quad (3)$$

where the  $\delta$  implies the variation of a variable. Requiring check-pointing Eq. (2) to be stationary with respect to  $\mathbf{w}$  recovers the primal problem from the second boxed term of check-pointing Eq. (3) with solution  $\mathbf{v} = \mathbf{u}_{ss}$ . Simultaneously requiring stationarity with respect to  $\mathbf{v}$ , the equation for the steady adjoint is obtained from the first boxed term of Eq. (3) with  $\mathbf{w} = \boldsymbol{\psi}_{ss}$ :

$$\mathbf{f}_{\mathbf{u}}(\mathbf{u}_{ss}; \beta)^T \boldsymbol{\psi}_{ss} - g_{\mathbf{u}}(\mathbf{u}_{ss}; \beta)^T = \mathbf{0} \quad (4)$$

where  $\boldsymbol{\psi}_{ss}$  is the steady adjoint variable. In the limit of small parameter variation, along with  $\mathbf{v} = \mathbf{u}_{ss}$  and  $\mathbf{w} = \boldsymbol{\psi}_{ss}$ , the parameter sensitivity of the output to  $\beta$  is given by

$$\frac{d\mathcal{J}}{d\beta} = \lim_{\delta\beta \rightarrow 0} \frac{\delta \mathcal{L}}{\delta \beta} = g_{\beta}(\mathbf{u}_{ss}; \beta) - \boldsymbol{\psi}_{ss}^T \mathbf{f}_{\beta}(\mathbf{u}_{ss}; \beta) \quad (5)$$

The steady flow is commonly solved using an iterative solver of the form

$$\mathbf{u}_{n+1} = \mathbf{u}_n - M_P(\mathbf{u}_n; \beta)^{-1} \mathbf{f}(\mathbf{u}_n; \beta) \quad (6)$$

where  $\mathbf{u}_n$  is the approximation to  $\mathbf{u}_{ss}$  at iteration  $n$  and  $M_P(\mathbf{u}_n; \beta)$  is a preconditioning matrix that approximates the Jacobian,  $\mathbf{f}_{\mathbf{u}}$ , evaluated at  $\mathbf{u}_n$ . Once Eq. (6) is acceptably converged, Eq. (4) can be solved via the fixed-point iteration:

$$\boldsymbol{\psi}_{m+1} = \boldsymbol{\psi}_m + M_P(\mathbf{u}_{ss}; \beta)^{-T} [g_{\mathbf{u}}(\mathbf{u}_{ss}; \beta)^T - \mathbf{f}_{\mathbf{u}}(\mathbf{u}_{ss}; \beta)^T \boldsymbol{\psi}_m] \quad (7)$$

The convergence rate of this fixed-point iteration for the adjoint is controlled by the eigenvalues of the matrix  $M_P(\mathbf{u}_{ss}; \beta)^{-T} \mathbf{f}_{\mathbf{u}}(\mathbf{u}_{ss}; \beta)^T$ . Note that as  $\mathbf{u}_n \rightarrow \mathbf{u}_{ss}$ , the convergence rate of Eq. (6) will be controlled by eigenvalues of  $M_P(\mathbf{u}_{ss}; \beta)^{-1} \mathbf{f}_{\mathbf{u}}(\mathbf{u}_{ss}; \beta)$ . Since  $\lambda(A^{-T}B^T) = \lambda(A^{-1}B)$ , unstable eigenvalues present in the primal iterative method will also be present in the adjoint iterative method.

### B. Unsteady Adjoint

Building on the steady adjoint method of sensitivity calculation, it is straightforward to derive an unsteady parameter sensitivity. First, the unsteady primal equations are

$$\begin{aligned} \mathbf{f}_e(\mathbf{u}, t; \beta) &= \mathbf{u}_t(t) + \mathbf{f}(\mathbf{u}(t); \beta) = \mathbf{0} \quad \forall t \in (0, t_f] \\ \mathbf{u}(0) &= \mathbf{u}^0 \end{aligned} \quad (8)$$

where  $\mathbf{u}(t): [0, t_f] \rightarrow \mathbb{R}^m$  is again the primal state vector. While in principle a more general output could be used, here we use the time average of the instantaneous output:

$$\mathcal{J}_e(\beta) = \frac{1}{t_f} \int_0^{t_f} g(\mathbf{u}(t); \beta) dt \quad (9)$$

The Lagrangian for the unsteady problem can then be defined as

$$\mathcal{L}_e(\mathbf{v}, \mathbf{w}; \beta) \equiv \frac{1}{t_f} \int_0^{t_f} \{g(\mathbf{v}(t); \beta) - \mathbf{w}(t)^T (\mathbf{v}_t(t) + \mathbf{f}(\mathbf{v}(t); \beta))\} dt \quad (10)$$

where  $\mathbf{v}, \mathbf{w}: [0, t_f] \rightarrow \mathbb{R}^m$ . As in the steady case, take the first variation with respect to the three arguments, and integrate appropriately by parts to get

$$\begin{aligned} \delta \mathcal{L}_e(\mathbf{v}, \mathbf{w}; \delta \mathbf{v}, \delta \mathbf{w}; \delta \beta) &= \frac{1}{t_f} \int_0^{t_f} \{ \delta \mathbf{v}(t)^T [g_{\mathbf{v}(t)}^T(\mathbf{v}(t); \beta) \\ &+ \mathbf{w}_t(t) - \mathbf{w}(t)^T \mathbf{f}_{\mathbf{v}(t)}(\mathbf{v}(t); \beta)] - \delta \mathbf{w}(t)^T [\mathbf{v}_t(t) + \mathbf{f}(\mathbf{v}(t); \beta)] \\ &+ \delta \beta^T [g_{\beta}^T(\mathbf{v}(t); \beta) - \mathbf{w}(t)^T \mathbf{f}_{\beta}(\mathbf{v}(t); \beta)] \} dt + \frac{1}{t_f} [\mathbf{w}(t)^T \delta \mathbf{v}(t)]_0^{t_f} \quad (11) \end{aligned}$$

Requiring stationarity with respect to  $\mathbf{w}$  and  $\mathbf{v}$  gives the primal and adjoint equations for  $\mathbf{v} = \mathbf{u}$  and  $\mathbf{w} = \boldsymbol{\psi}$ , respectively. Specifically, the unsteady adjoint equation is

$$-\boldsymbol{\psi}_t(t) + \mathbf{f}_u(\mathbf{u}(t); \beta)^T \boldsymbol{\psi}(t) - g_u(\mathbf{u}(t); \beta)^T = \mathbf{0} \quad \forall t \in [0, t_f] \quad (12)$$

For a fixed initial flow state and thus a zero initial variation,  $\delta \mathbf{v}(0) = \mathbf{0}$ , the final term gives the adjoint terminal condition:

$$\boldsymbol{\psi}(t_f) = \mathbf{0} \quad (13)$$

The adjoint equation must be solved in reverse time, which is clear from the terminal equation (13) and the sign of the  $\boldsymbol{\psi}_t$  term compared to the second term of Eq. (12). The dependence of the second and third terms in the primal solution then requires the full storage or recalculation via check-pointing of the primal through the time span of interest.

As in the steady case, the parameter sensitivity for unsteady problems,  $d\mathcal{J}_e/d\beta$ , is determined from the variation of Lagrangian in the limit of small parameter variation:

$$\frac{d\mathcal{J}_e}{d\beta} = \lim_{\delta\beta \rightarrow 0} \frac{\delta \mathcal{L}_e}{\delta \beta} = \frac{1}{t_f} \int_0^{t_f} \{g_{\beta}(\mathbf{u}(t); \beta) - \boldsymbol{\psi}(t)^T \mathbf{f}_{\beta}(\mathbf{u}(t); \beta)\} dt \quad (14)$$

### C. Discrete Unsteady Adjoint

In this work, we use a fourth-order-accurate explicit singly diagonal implicit Runge–Kutta (ESDIRK) time-stepping scheme for the computational examples, but in order to simplify the analysis we will use the first-order backward difference for comparison against the steady adjoint iteration:

$$\begin{aligned} \tilde{\mathbf{f}}_e(\mathbf{u}, n; \beta) &= \frac{\mathbf{u}_{n+1} - \mathbf{u}_n}{\Delta t} + \mathbf{f}(\mathbf{u}_{n+1}; \beta) = \mathbf{0} \quad \forall n \in [0, N-1] \\ \mathbf{u}_0 &= \mathbf{u}^0 \end{aligned} \quad (15)$$

where  $N$  is the number of time steps spanning the time span of interest, with a constant time step  $\Delta t = t_f/N$ . Deriving the time integration of the output from the time-stepping scheme of the primal problem gives

$$J_e = \frac{\Delta t}{t_f} \sum_{n=1}^N g(\mathbf{u}_n; \beta) \quad (16)$$

The discrete Lagrangian can then be defined by

$$L_e(\mathbf{v}, \mathbf{w}; \beta) = \frac{\Delta t}{t_f} \sum_{n=1}^N \left\{ g(\mathbf{v}_n; \beta) - \mathbf{w}_n^T \left[ \frac{\mathbf{v}_n - \mathbf{v}_{n-1}}{\Delta t} + \mathbf{f}(\mathbf{v}_n; \beta) \right] \right\} \quad (17)$$

Enforcing stationarity of the discrete Lagrangian with respect to  $\mathbf{w}_n$   $\forall n \in [1, N+1]$  and  $\mathbf{v}_n$   $\forall n \in [0, N]$  gives the discrete adjoint equation for  $\mathbf{w}_n = \boldsymbol{\psi}_n$ :

$$\begin{aligned} \frac{\boldsymbol{\psi}_n - \boldsymbol{\psi}_{n+1}}{\Delta t} + \mathbf{f}_u(\mathbf{u}_n; \beta)^T \boldsymbol{\psi}_n - g_u^T(\mathbf{u}_n; \beta) &= \mathbf{0} \quad \forall n \in [1, N] \\ \boldsymbol{\psi}_{N+1} &= \mathbf{0} \end{aligned} \quad (18)$$

In contrast to Eq. (7), the linearization and output derivative in the unsteady adjoint equation are taken about the primal state at successive time instants, rather than at a fixed point. This stabilizes the calculation, and stability no longer depends on the eigenvalues of  $\Delta t \mathbf{f}_u(\mathbf{u}_n; \beta)^T$  being within the unit circle at a particular time step. Equation (18) can now be used to compute the adjoint even about unstable stationary points.

The parameter sensitivity for the first-order backward difference is derived as in the continuous case:

$$\frac{dJ_e}{d\beta} = \frac{\Delta t}{t_f} \sum_{n=1}^N \{g_{\beta}(\mathbf{u}_n; \beta) - \boldsymbol{\psi}_n^T \mathbf{f}_{\beta}(\mathbf{u}_n; \beta)\} \quad (19)$$

## III. Model Problem and Discretization

### A. Equations and Discretization

The time-dependent compressible Navier–Stokes equations are given by

$$\frac{\partial \mathbf{u}}{\partial t} + \nabla \cdot \mathcal{F}_i(\mathbf{u}) - \nabla \cdot \mathcal{F}_v(\mathbf{u}, \nabla \mathbf{u}) = \mathbf{0} \quad (20)$$

In two dimensions, the state vector is given by  $\mathbf{u} = [\rho, \rho u, \rho v, \rho e]^T$ .  $\mathcal{F}_i(\mathbf{u})$  and  $\mathcal{F}_v(\mathbf{u}, \nabla \mathbf{u})$  are the inviscid and viscous flux vectors, respectively. The discontinuous Galerkin (DG) discretization of the Navier–Stokes equations is obtained by choosing a triangulation  $\mathcal{T}_H$  of the computational domain  $\Omega$  composed of triangular elements  $\kappa$ , and obtaining a solution  $\mathbf{u}_H$  that satisfies the weak form of the equation in the space  $\mathcal{V}_H^p$ :

$$\begin{aligned} \mathcal{V}_H^p &= \{ \mathbf{v} = [v_1, \dots, v_m]^T | v_i \in L^2(\Omega), v_i|_{\kappa} \in P^p(\kappa) \\ &\forall \kappa \in \mathcal{T}_H, i = 1, \dots, m \} \end{aligned}$$

where  $P^p(\kappa)$  the space of polynomials of order  $p$  on element  $\kappa$ . The discrete solution vector can be expressed as a linear combination of basis functions,  $\mathbf{v}_{H_i} \in \mathcal{V}_H^p$ :

$$\mathbf{u}_H(x, t) = \sum_i \mathbf{U}_{H_i}(t) \mathbf{v}_{H_i}(x) \quad (21)$$

where  $\mathbf{U}_H$  is the vector of basis coefficients for the finite element basis. The weak form is obtained by taking the inner product of Eq. (20) and a test function  $\mathbf{v}_H \in \mathcal{V}_H^p$  and integrating over all elements in the triangulation of the domain:

$$\sum_{\kappa \in \mathcal{T}_H} \int_{\kappa} \mathbf{v}_H^T \frac{\partial \mathbf{u}_H}{\partial t} + \mathcal{R}_H(\mathbf{u}_H, \mathbf{v}_H; \beta) = \mathbf{0} \quad \forall \mathbf{v}_H \in \mathcal{V}_H^p \quad (22)$$

where  $\mathcal{R}_H$  is a semilinear form composed of the spatial discretizations of inviscid and viscous terms. Specifically, the inviscid flux between elements is resolved using the Roe flux [26] and the viscous terms are discretized using the second method of Bassi and Rebay [27]. The spatially discrete unsteady primal Navier–Stokes equations are given by

$$\mathcal{M} \frac{d\mathbf{U}_H}{dt} + \mathbf{R}_H(\mathbf{U}_H; \beta) = \mathbf{0} \quad (23)$$

where  $\mathbf{R}_H$  is the discrete spatial nonlinear residual such that  $\mathbf{R}_{H_i}(\mathbf{U}_H) = \mathcal{R}_H(\mathbf{u}_H, \mathbf{v}_{H_i})$ , and  $\mathcal{M}$  is the mass matrix given by

$$\mathcal{M}_{ij} = \int_{\kappa} \mathbf{v}_{H_i} \mathbf{v}_{H_j} d\Omega_{\kappa} \quad (24)$$

The adjoint equation is

$$-\mathcal{M} \frac{d\boldsymbol{\Psi}_H}{dt} + \left[ \frac{\partial \mathbf{R}_H(\mathbf{U}_H; \beta)}{\partial \mathbf{U}_H} \right]^T \boldsymbol{\Psi}_H - \frac{\partial J(\mathbf{U}_H; \beta)^T}{\partial \mathbf{U}_H} = \mathbf{0} \quad (25)$$

and parameter sensitivity is given by

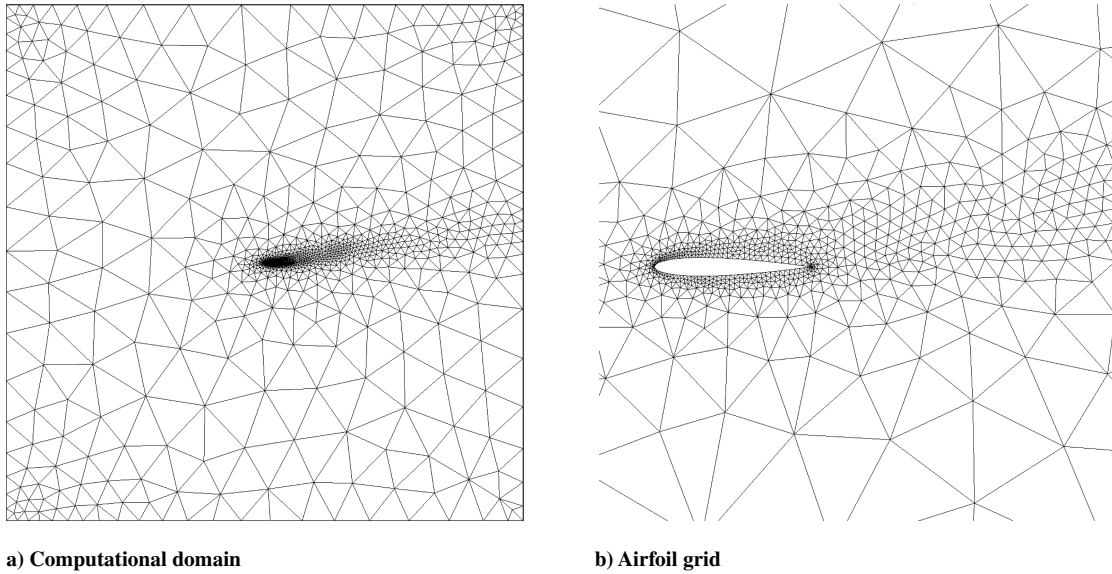
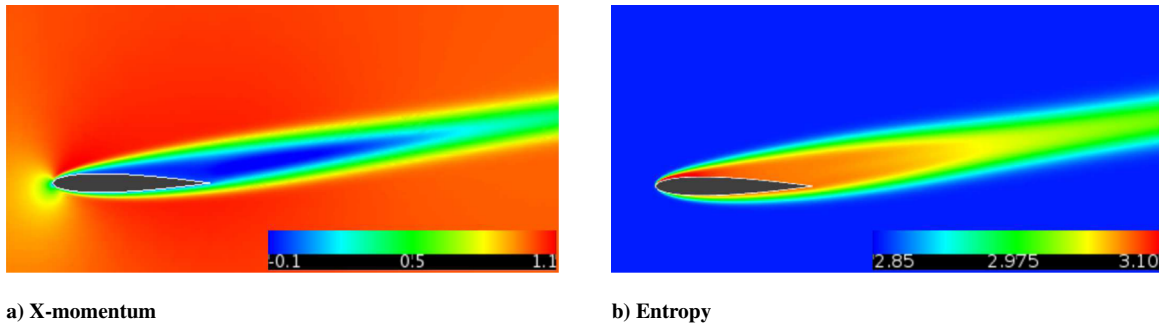


Fig. 1 NACA 0012 mesh.

Fig. 2 NACA 0012, GMRES stationary-point solution ( $Ma = 0.5$ ,  $Re = 1500$ , and  $\alpha = 9^\circ$ ).

$$\frac{dJ_e}{d\beta} = \frac{1}{t_f} \int_0^{t_f} \left\{ \frac{\partial J(\mathbf{U}_H; \beta)}{\partial \beta} - \Psi_H^T \frac{\partial \mathbf{R}_H(\mathbf{U}_H; \beta)}{\partial \beta} \right\} dt \quad (26)$$

The only unsteady addition for the DG form is the inclusion of the mass matrix  $\mathcal{M}$  in the temporal terms, the result being that the individual components that come from the unsteady terms are now premultiplied by the mass matrix.

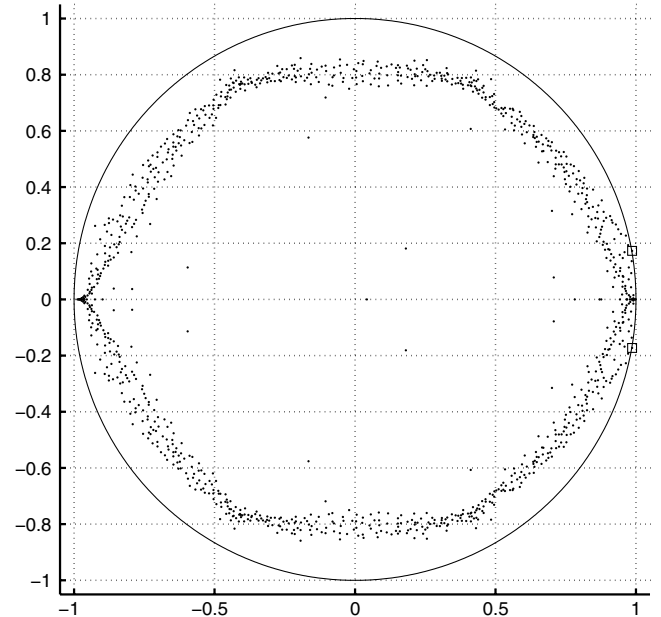
### B. Nonlinear and Linear Solvers

For steady, i.e., time-inaccurate, simulations, Newton's method is used with backward Euler pseudo time stepping to increase robustness during transients. The pseudo time step in each element is governed by the Courant–Friedrichs–Lewy (CFL) number. For uniform flow initial conditions the simulation is started with  $CFL = 1$  and allowed to increase (by factors of 2) as long as the flow solution maintains positive density and pressure, up to a maximum  $CFL_{\max} = 10^{30}$ . All time-inaccurate results are reported after the CFL has reached  $CFL_{\max}$ .

For time-accurate simulations, the temporal derivative term is discretized with a fourth-order ESDIRK scheme [28]. At each time step (and stage of the ESDIRK scheme) the same Newton's method as for time-inaccurate problems is used to converge the unsteady primal equation (23). The discrete adjoint was derived using the methods of Sec. II.C, but with the additional complexity of the multistage ESDIRK scheme.

The linear systems arising in both the time-inaccurate and time-accurate simulations were solved with stationary iterative methods (block-Jacobi and line-Jacobi) either as the solver or as a preconditioner for GMRES [29]. At each iteration, the block-Jacobi method solves for the degrees of freedom within each element as a block. The line-Jacobi stationary iterative method expands the size of

the block, solving within a line of elements. As a result, the stationary iterative methods are most effective at reducing errors within blocks (i.e., local errors). The GMRES solver uses a Krylov subspace that is computed over the entire flow domain, incorporating more than

Fig. 3 Eigenvalues of line-preconditioned iterative system ( $I - \mathcal{M}^{-1}R_U$ ) at stationary point ( $Ma = 0.5$ ,  $Re = 1500$ ,  $\alpha = 9^\circ$ , and four processors).

nearest-neighbor dependence, and making it more effective at reducing global errors. Unlike the stationary iterative methods, GMRES is guaranteed to converge monotonically, regardless of the presence of outlier (unstable) modes, for any nonsingular matrix. Because the GMRES linear solver does not have the same susceptibility as the stationary iterative methods to unstable modes, it is capable of computing a stationary-point solution if one exists, whether or not the stationary-point solution is stable.

For time-inaccurate problems, a simulation is considered converged if the  $L_2$  norm of spatial residual is decreased by 10 orders of magnitude from its initial value. For time-accurate problems, the same criterion is used for the unsteady residual, with the additional temporal terms, of each time step and time-step stage.

**C. Model Problem**

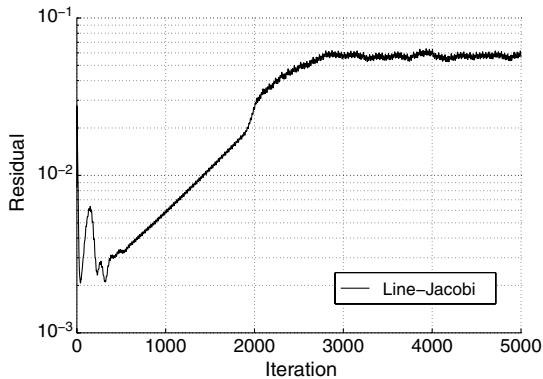
Subsonic laminar flow about an airfoil is used to demonstrate the impact of small-scale output unsteadiness on sensitivity analysis. Specifically, we consider the  $Ma = 0.5$  and  $Re = 1500$  flow about a two-dimensional NACA 0012 airfoil over a range of angles of attack. This problem was chosen because the flowfield exhibits a stable stationary point at lower angles of attack, but for higher angles of attack, it has an unstable stationary point, leading to unsteady

behavior. In the computational mesh, the airfoil leading edge is located at  $(0, 0)$  with a unit chord. The domain is square and extends  $[-10, 10] \times [-10, 10]$ . The mesh refinement was determined using adjoint-based adaptation, driving the error in lift coefficient  $C_L$  to less than 0.0005 for a  $p = 3$  stationary-point solution at integer angles of attack from  $\alpha = 0$  to  $13^\circ$ . For the problems in this work, a mesh was generated with 2158 elements, shown in Fig. 1. The resulting airfoil surface is defined by 101 nodes, connected by cubic polynomial edges ( $q = 3$ ), with the endpoint and edge nodes projected to the analytic geometry. In this work, the flow and adjoint states are represented in each element by a polynomial of degree 3 ( $p = 3$ ). For time-accurate unsteady problems, a time step of 0.1 with units based on the freestream velocity is used with the ESDIRK4 temporal discretization. A grid and time-step dependence study was done and is discussed in Appendix A.

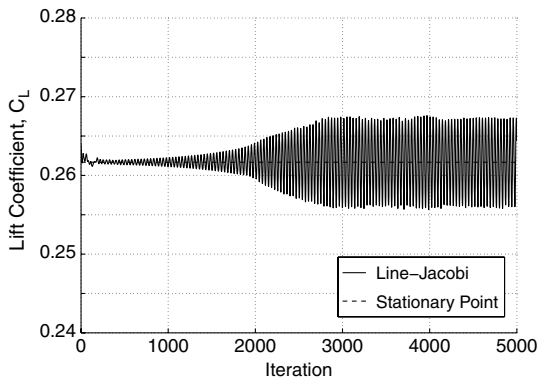
**IV. Time-Inaccurate Simulations**

**A. Nine-Degree Angle of Attack**

For freestream conditions  $Ma = 0.5$  and  $Re = 1500$ , a stationary-point solution of a NACA 0012 airfoil at a  $9^\circ$  angle of attack can be found using a line-Jacobi preconditioned GMRES linear solver. This stationary-point solution exhibits a large laminar separation region,

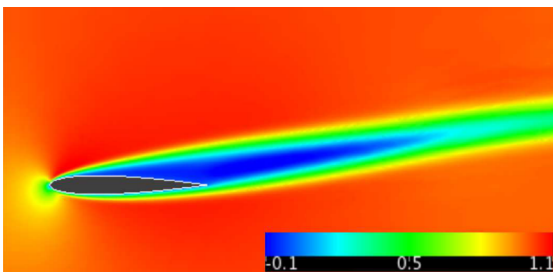


a) Residual history

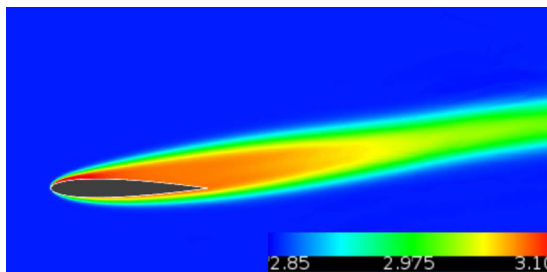


b) Lift coefficient history

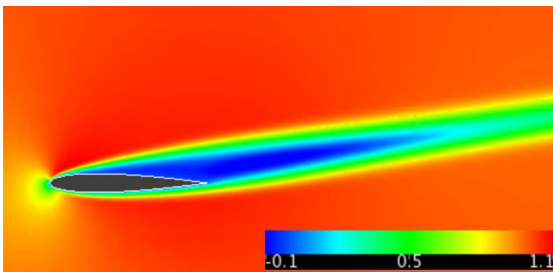
**Fig. 4** Convergence history for line Jacobi ( $Ma = 0.5$ ,  $Re = 1500$ ,  $\alpha = 9^\circ$ , and four processors).



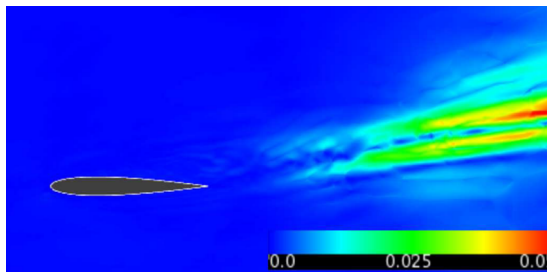
a) X-momentum snapshot



b) Entropy snapshot



c) X-momentum mean



d) X-momentum standard deviation

**Fig. 5** NACA 0012, line-Jacobi iterative solver ( $Ma = 0.5$ ,  $Re = 1500$ , and  $\alpha = 9^\circ$ ).

shown in Fig. 2. For weaker linear solvers, such as line-Jacobi without GMRES, the eigenvalues of the linear system lie outside the stability region, which is a unit circle centered at the origin. Specifically, the eigenvalues for the linear system at the stationary point of the line-Jacobi preconditioned system  $(I - \mathcal{M}^{-1}R_U)$  are shown in Fig. 3. These eigenvalues were calculated using a Krylov subspace of 1000 vectors, giving 1000 eigenvalues. Since there are eigenvalues outside the unit circle (denoted by the squares), the line-Jacobi iterative method will be unstable for the linearized primal as well as the adjoint problem. Further, this instability will also prevent the nonlinear primal iteration from converging to the stationary point. As shown in Fig. 4, when the line-Jacobi iterative solver is started from the prolonged  $p = 2$  stationary-point solution, the nonlinear residual is initially  $\sim 10^{-3}$ , but immediately begins rising until it reaches an equilibrium at  $\sim 0.06$ . Likewise, the lift does not converge to a single value but has a small-amplitude time-inaccurate unsteadiness with a mean near the value of the stationary point. After the transients have diminished, the standard deviation of  $C_L$  from the mean is approximately 1.5% of the stationary-point value.

To examine the time-inaccurate unsteadiness in the line-Jacobi solution further, the transient was allowed to die out, and the mean and the standard deviation of the time-inaccurate solution were calculated over 50,000 iterations. The standard deviation of each

component of the state was computed by using a Lagrange basis and calculating the value at each Lagrange point. At a Lagrange point  $i$ , the mean is computed as

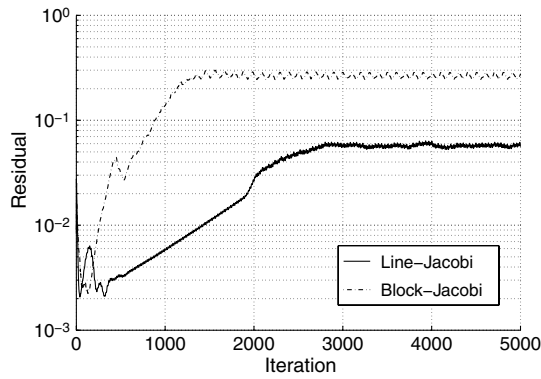
$$\bar{u}^i = \frac{1}{N} \sum_{n=1}^N u_n^i$$

and the standard deviation is computed as

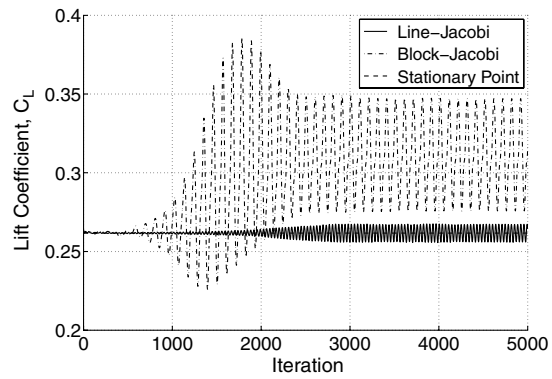
$$\sigma^i(\mathbf{u}) = \left[ \frac{1}{N} \sum_{n=1}^N (u_n^i - \bar{u}^i)^2 \right]^{1/2}$$

The mean and standard deviation of the  $x$  momentum are plotted in Fig. 5. The standard deviation in the  $x$  momentum is representative of the variation of all of the states, with a maximum magnitude of approximately 6% of the mean flow on the laminar separation bubble boundary.

The time-inaccurate unsteady behavior in this case is highly dependent on the strength of the iterative solver. For stationary iterative solvers, time-inaccurate unsteadiness begins to appear in the wake region, one–two chords downstream, as shown in Fig. 5d. Regardless, the mean flow near the airfoil appears almost identical to

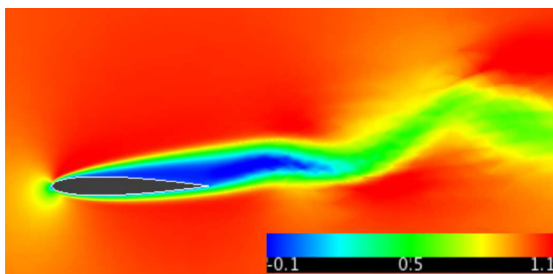


a) Residual history

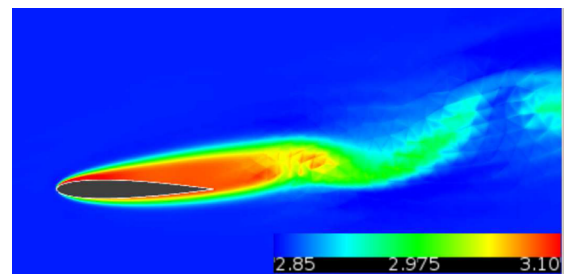


b) Lift coefficient history

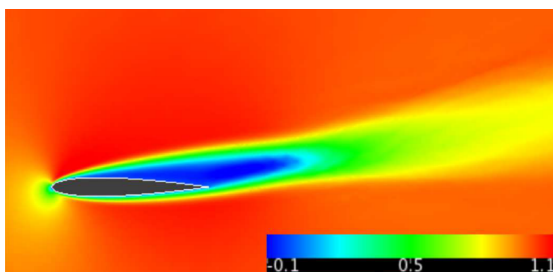
Fig. 6 Convergence history for block Jacobi ( $Ma = 0.5$ ,  $Re = 1500$ , and  $\alpha = 9^\circ$ ).



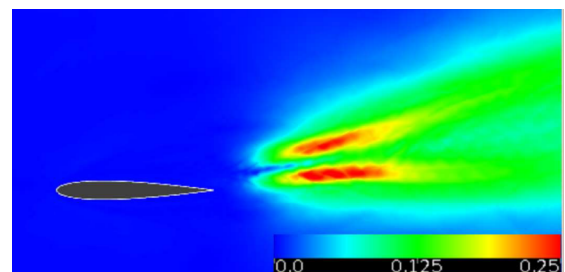
a) X-momentum snapshot



b) Entropy snapshot



c) X-momentum mean



d) X-momentum standard deviation

Fig. 7 NACA 0012, block-Jacobi iterative solver ( $Ma = 0.5$ ,  $Re = 1500$ , and  $\alpha = 9^\circ$ ).

the stationary point, as in a comparison of Figs. 2a and 5c. Replacing the line-Jacobi iterative solver with a block-Jacobi solver decreases the strength of the preconditioning. The convergence history for the same conditions, but with the weaker solver, is shown in Fig. 6, exhibiting larger time-inaccurate unsteadiness in the output as well as a different mean value. The mean and standard deviation of the  $x$  momentum are plotted in Fig. 7, showing an increase in the magnitude of the standard deviation in the wake. The  $x$  momentum and entropy snapshots show large unsteadiness in the wake, with an indication of vortex shedding into the wake (though we emphasize that this is not a time-accurate simulation).

Returning to the line-Jacobi iterative results, one could reasonably presume from the low variation in the lift coefficient that linearizing about an iterate of the unconverged primal is sufficient to provide accurate lift sensitivity estimates. However, the derivation of the adjoint-based sensitivity depends on the stationarity of the

Lagrangian with respect to variation of the adjoint. When the spatial residual is not zero for the primal state about which the adjoint analysis is performed, the output sensitivity has an additional term. Examination of Eq. (3) shows that the output sensitivity then becomes dependent on the inner product of the residual and the derivative of the adjoint with respect to the parameter. To demonstrate the impact that using an unconverged solution can have on the sensitivity analysis, we use a stronger linear solver [GMRES preconditioned with incomplete LU (ILU) factorization with zero introduced fill] to perform adjoint analysis by linearizing about iterates  $u_n$  for a series of iterations  $n$ . As shown in Fig. 8, this estimate of  $dC_L/d\alpha$  (i.e.,  $g = C_L$  and  $\beta = \alpha$ ) varies over a range from 0.519 to 0.639  $\text{rad}^{-1}$ . Depending on the iterate used in the linearization, the sensitivity from an unconverged state could be significantly different from the sensitivity computed about the stationary point (0.558  $\text{rad}^{-1}$ ). Taking the average of these iterate sensitivities gives

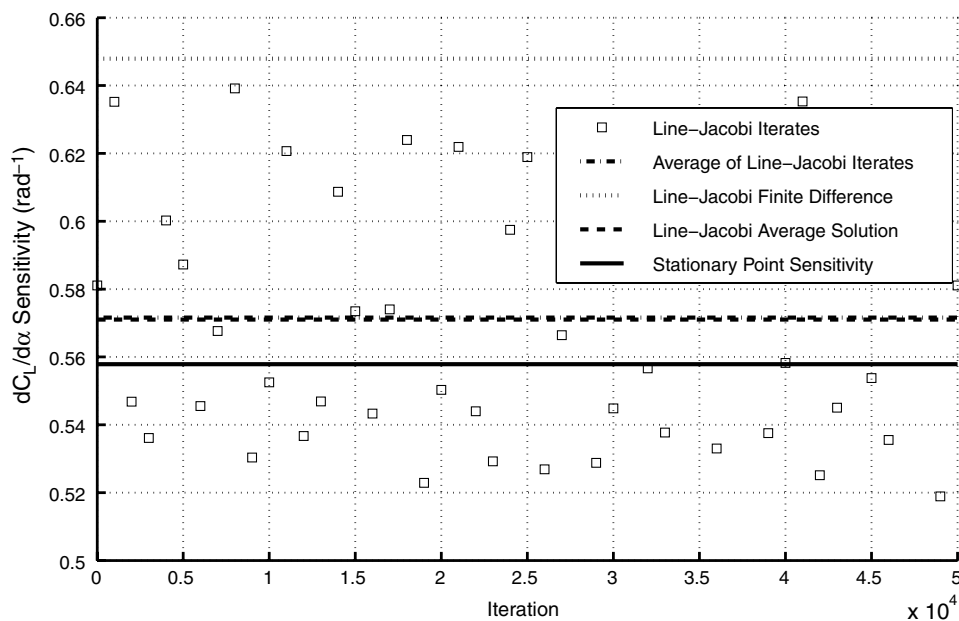


Fig. 8 Comparison of  $dC_L/d\alpha$  at  $\alpha = 9^\circ$ .

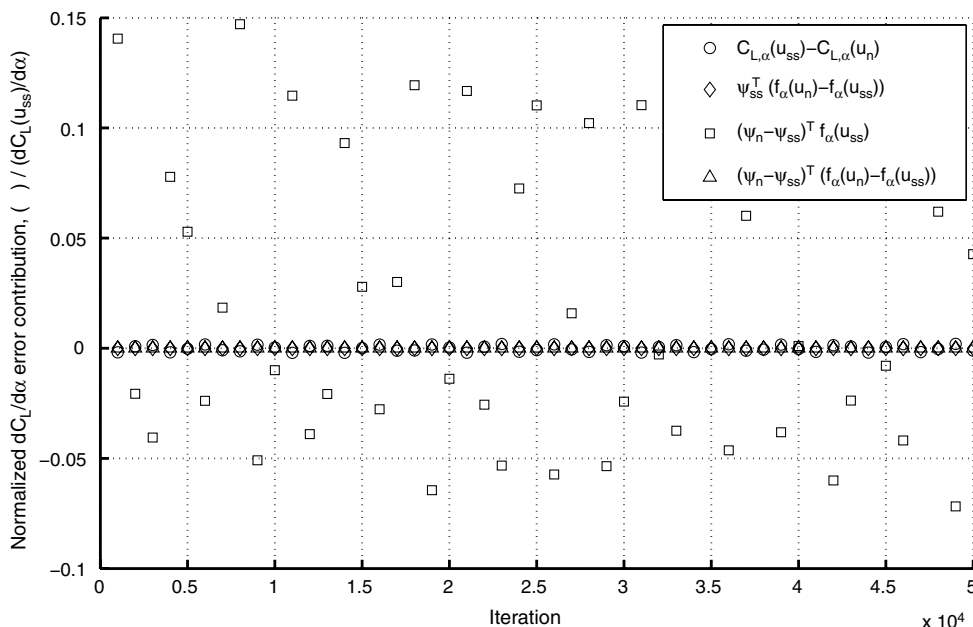


Fig. 9 Time-inaccurate sensitivity error terms, normalized by stationary-point sensitivity,  $\alpha = 9^\circ$ .

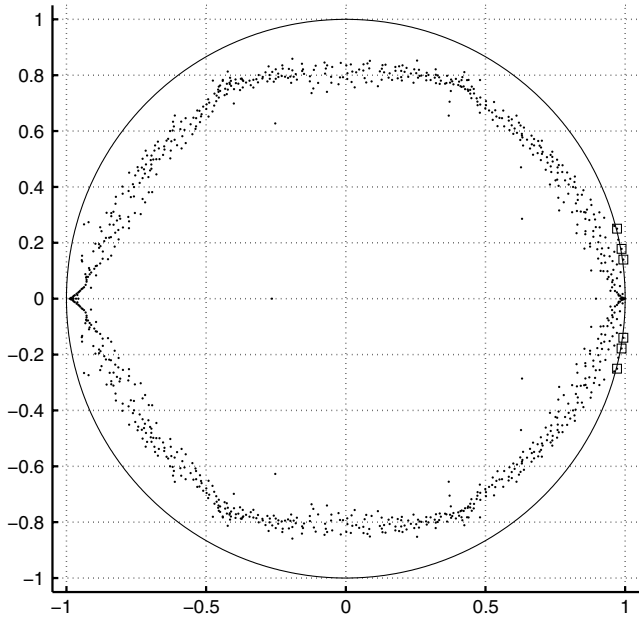


Fig. 10 Eigenvalues of line-preconditioned iterative system ( $I - \mathcal{M}^{-1}R_U$ ) at stationary point ( $Ma = 0.5$ ,  $Re = 1500$ ,  $\alpha = 10^\circ$ , and four processors).

$0.571 \text{ rad}^{-1}$ , which is within  $\sim 2.3\%$  of the stationary-point sensitivity. When the GMRES linear solver is used to calculate the output sensitivity of the iteration average of the line-Jacobi solutions, the sensitivity is  $0.571 \text{ rad}^{-1}$ , matching the average of the iterate sensitivities. The usefulness of these sensitivities is limited, as they all required the stronger GMRES solver to compute the adjoint, which could then have been available to solve for the stationary flow solution. Finally, perturbing the angle of attack by  $\pm 0.01^\circ$  and calculating a central difference of the averages of the lift over the range of iterations plotted in Fig. 8 gives a sensitivity of  $0.648 \text{ rad}^{-1}$ , which is approximately 16% greater than the stationary-point sensitivity.

To determine the sources of error in the sensitivity when the iterative solvers are used, the difference between the iterate and stationary-point sensitivities is decomposed into four terms:

$$\begin{aligned} \frac{d\mathcal{J}(\mathbf{u}_n)}{d\beta} - \frac{d\mathcal{J}(\mathbf{u}_{ss})}{d\beta} &= [g_\beta(\mathbf{u}_n; \beta) - g_\beta(\mathbf{u}_{ss}; \beta)] \\ &\quad - [\boldsymbol{\psi}_{ss}^T (\mathbf{f}_\beta(\mathbf{u}_n; \beta) - \mathbf{f}_\beta(\mathbf{u}_{ss}; \beta))] - [(\boldsymbol{\psi}_{u_n} - \boldsymbol{\psi}_{ss})^T \mathbf{f}_\beta(\mathbf{u}_{ss}; \beta)] \\ &\quad - [(\boldsymbol{\psi}_{u_n} - \boldsymbol{\psi}_{ss})^T (\mathbf{f}_\beta(\mathbf{u}_n; \beta) - \mathbf{f}_\beta(\mathbf{u}_{ss}; \beta))] \end{aligned} \quad (27)$$

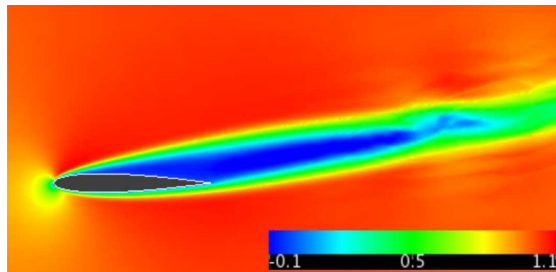
Figure 9 shows the four contributing error terms for the same line-Jacobi iterate snapshots shown in Fig. 8. Each term is normalized by the stationary-point sensitivity. The adjoint error term,  $(\boldsymbol{\psi}_{u_n} - \boldsymbol{\psi}_{ss})^T \mathbf{f}_\beta(\mathbf{u}_{ss}; \beta)$ , causes almost the entire error, with contributions from the other terms negligible in comparison. This suggests that a correction method that depends on the contribution of the adjoint variation being small will not provide an accurate correction and that computing an accurate adjoint is paramount.

### B. Ten-Degree Angle of Attack

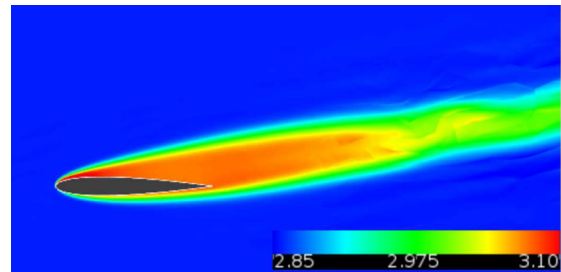
For the same freestream conditions,  $Ma = 0.5$  and  $Re = 1500$ , a stationary-point solution of the NACA 0012 airfoil can be computed at a  $10^\circ$  angle of attack. This stationary-point solution is qualitatively identical to the stationary point at  $\alpha = 9^\circ$ , shown in Fig. 2. The eigenvalues for the line-preconditioned linear system computed at the stationary point are shown in Fig. 10. In comparison with the eigenvalues at  $\alpha = 9^\circ$ , the number of unstable eigenvalues (denoted by the squares) has increased, indicating that the instability has increased with angle of attack.

The increase in time-inaccurate unsteadiness is verified in Fig. 11; the momentum and entropy snapshots show a visible disturbance in the wake and the largest magnitude of the momentum standard deviation is three times the  $\alpha = 9^\circ$  value. When the weaker block-Jacobi solver is used, the increase in time-inaccurate unsteadiness is even more pronounced. Figure 12d shows a large area of unsteadiness approximately one chord downstream. Even though this is not a time-accurate simulation, the  $x$  momentum and entropy snapshots now clearly indicate the shedding of vortices in the wake.

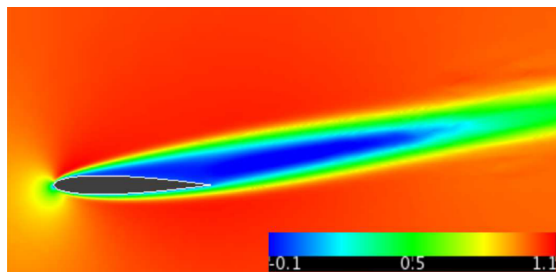
The residual and  $C_L$  iteration histories in Fig. 13 also show the increase in time-inaccurate unsteady behavior. The residual equilibrates at a higher value for either the block- or line-Jacobi iterative solver. For the line-Jacobi solver, the time-inaccurate standard deviation of  $C_L$  is approximately 3.0% of the stationary point  $C_L$  (twice the standard deviation with the same solver at  $\alpha = 9^\circ$ ).



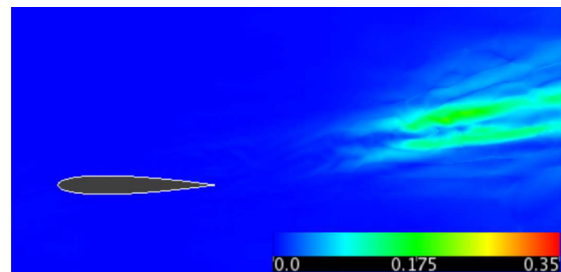
a) X-momentum snapshot



b) Entropy snapshot



c) X-momentum mean



d) X-momentum standard deviation

Fig. 11 NACA 0012, line-Jacobi iterative solver ( $Ma = 0.5$ ,  $Re = 1500$ , and  $\alpha = 10^\circ$ ).

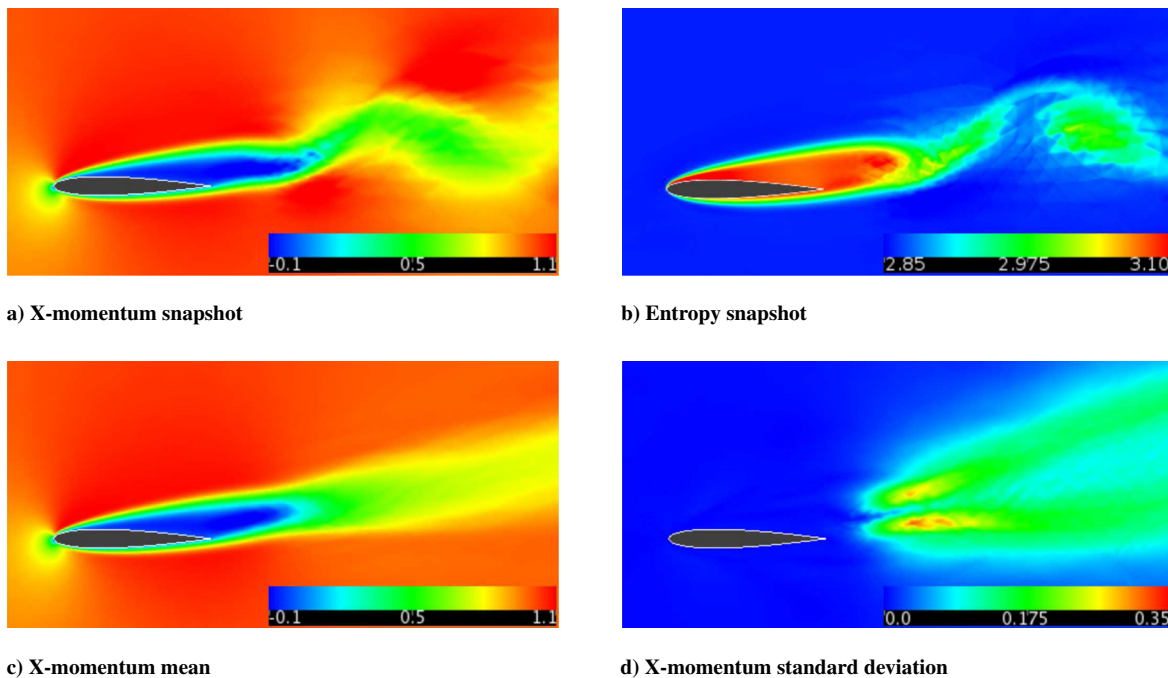


Fig. 12 NACA 0012, block-Jacobi iterative solver ( $Ma = 0.5$ ,  $Re = 1500$ , and  $\alpha = 10^\circ$ ).

At a  $9^\circ$  angle of attack, the sensitivities computed at individual iterate solutions vary by as much as 15% from the stationary-point sensitivity, but the averaging methods provide sensitivities within 2.3%. One might expect that at  $\alpha = 10^\circ$  by doubling the variation in  $C_L$  that the unsteadiness in the sensitivities would increase by a similar amount. This assumption is investigated in Fig. 14. At  $\alpha = 10^\circ$  the  $dC_L(\mathbf{u}_n)/d\alpha$  varies from 0.175 to 1.318  $\text{rad}^{-1}$ , which is significantly larger range than computed at  $\alpha = 9^\circ$ . The average of these iterate sensitivities gives 0.760  $\text{rad}^{-1}$ , which is again significantly different than the stationary-point sensitivity of 0.499  $\text{rad}^{-1}$ . When the GMRES linear solver is used to calculate the output sensitivity of the iteration average of the line-Jacobi solutions, the sensitivity is 0.707  $\text{rad}^{-1}$ . Finally, a central difference of  $C_L(\mathbf{u}_n)$  with  $\pm 0.01^\circ$  angle-of-attack perturbations gives a sensitivity of 1.015  $\text{rad}^{-1}$ , more than twice the stationary-point sensitivity.

### V. Time-Accurate Simulations

The flowfield about the airfoil when calculated using a time-accurate fourth-order ESDIRK scheme shows a character markedly different from the stationary-point solution from the time-inaccurate iterative approach. Figure 15 shows the unsteady behavior of the output for a case started near the stationary-point solution, the same

initial condition as was used for the line-Jacobi iterative method in the time-inaccurate analysis. A snapshot of that flow as well as the mean X momentum and the standard deviation of the X momentum state are shown in Fig. 16. The output suggests, and the snapshots clearly show, that the time-accurate flow has a series of alternating vortices shedding into the wake. This difference is reflected in the lift, almost doubling it compared to the stationary point. Further comparison of the time-accurate behavior against stationary-point solutions over an angle-of-attack sweep shows that the time-accurate unsteady behavior is not only dominant at  $\alpha = 10^\circ$ , but that unsteadiness begins somewhere between  $\alpha = 4$  and  $5^\circ$ , shown in Fig. 17. To compute the stationary-point solutions, the ILU preconditioned GMRES solver was used to compute all angles of attack in the sweep. Alternately, when the element block-Jacobi iterative solver was employed it converged below  $\alpha = 8^\circ$ , while the line-Jacobi solver across four processors converged below  $\alpha = 9^\circ$ . This implies that the ability to achieve a stationary-point solution does not guarantee that no physical unsteady behavior exists or, if it does exist, that it is even small.

Given the significant difference between the stationary-point and time-accurate solutions, reliable sensitivity analysis for flows that could exhibit unsteadiness must clearly be based on a time-accurate approach. To demonstrate this time-accurate adjoint analysis, the

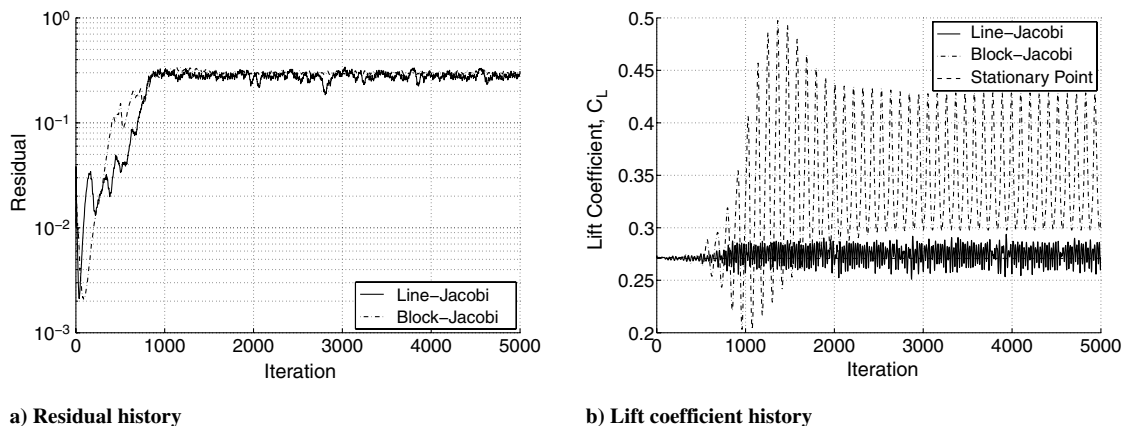


Fig. 13 Convergence history for block and line Jacobi ( $Ma = 0.5$ ,  $Re = 1500$ , and  $\alpha = 10^\circ$ ).

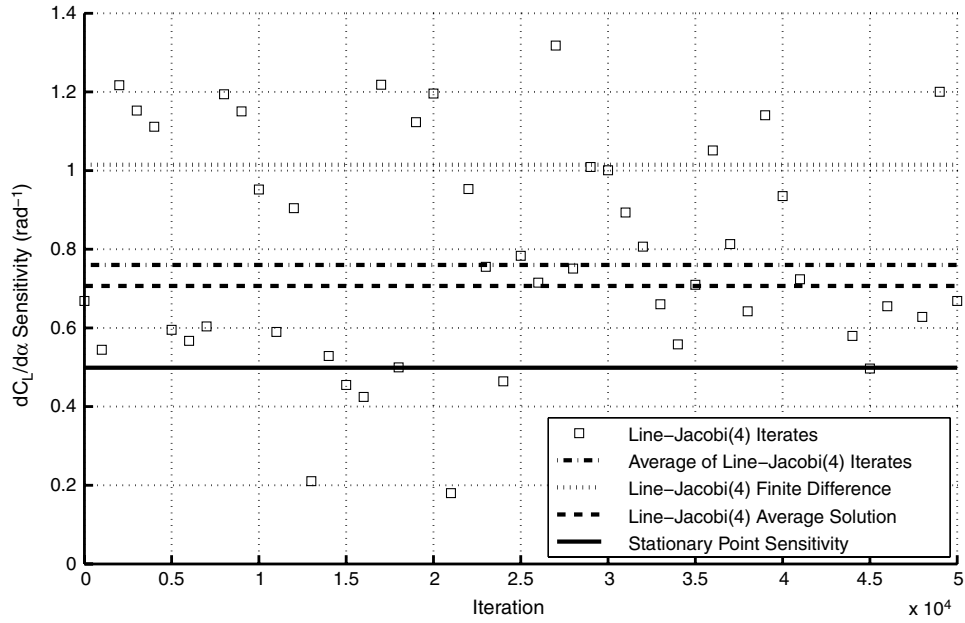


Fig. 14 Comparison of  $dC_L/d\alpha$  at  $\alpha = 10^\circ$ .

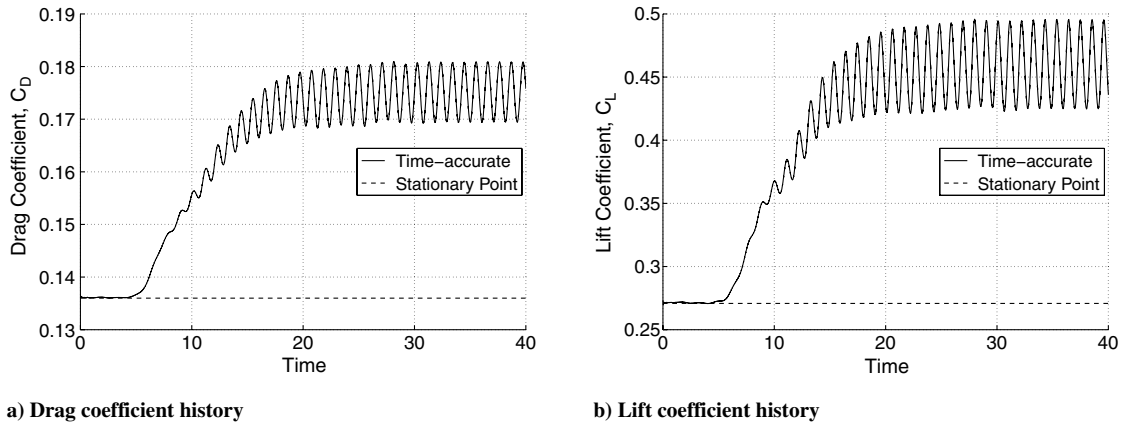
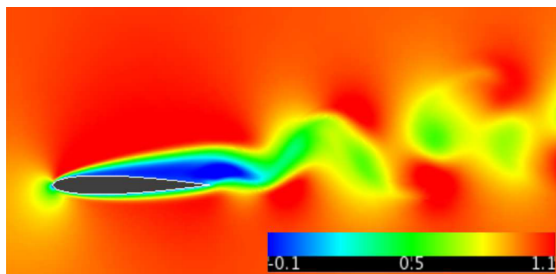
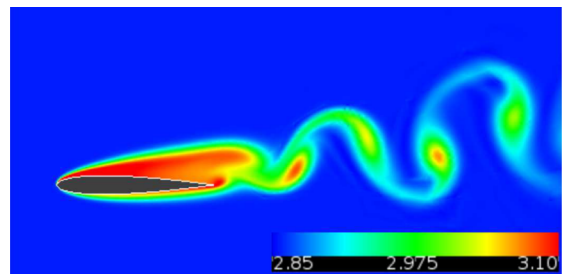


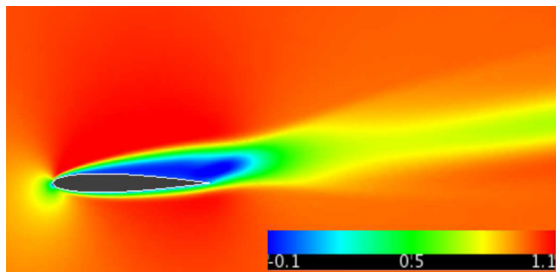
Fig. 15 Force output for unsteady NACA 0012 ( $Ma = 0.5$ ,  $Re = 1500$ , and  $\alpha = 10^\circ$ ).



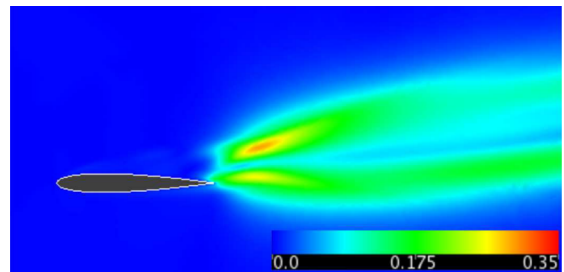
a) X-momentum snapshot



b) Entropy snapshot



c) X-momentum mean ( $t=100 \dots 200$ )



d) X-momentum standard deviation ( $t=100 \dots 200$ )

Fig. 16 NACA 0012, time-accurate solution ( $Ma = 0.5$ ,  $Re = 1500$ , and  $\alpha = 10^\circ$ ).

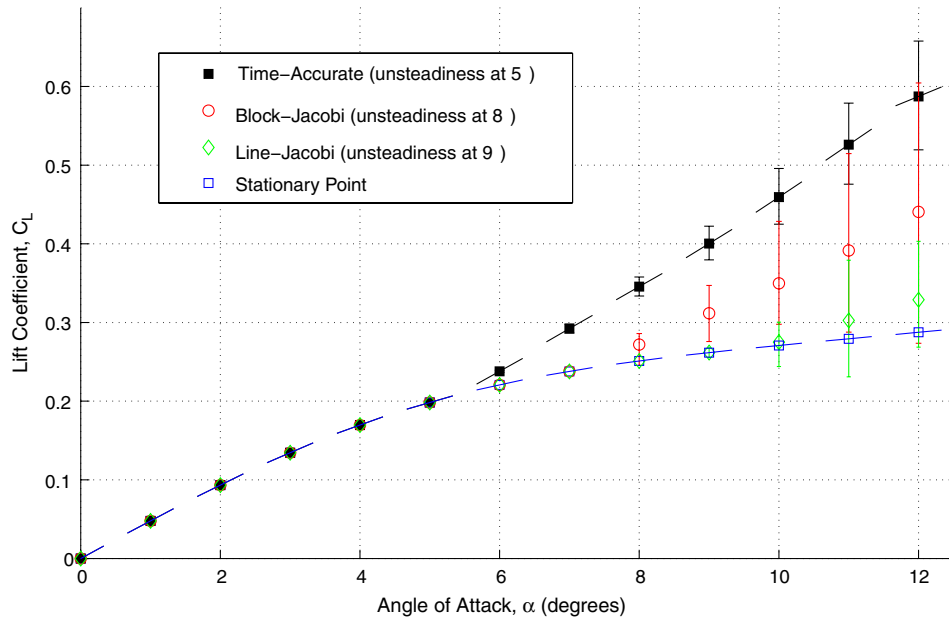


Fig. 17 NACA 0012 steady and time-accurate unsteady lift slope curve (dashes show  $dC_L/d\alpha$ ; error bars show minimum and maximum).

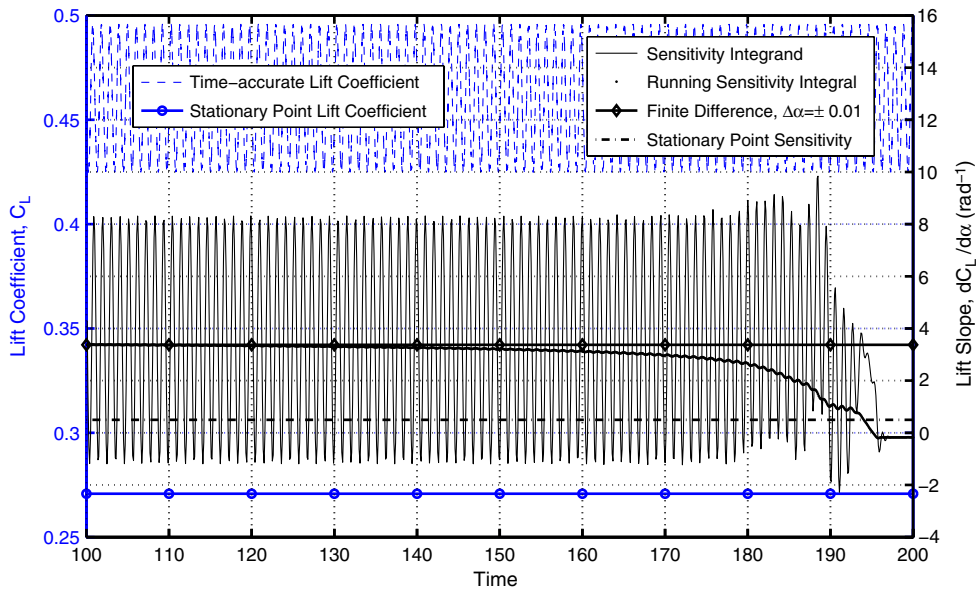


Fig. 18 Unsteady sensitivity convergence history of  $dC_L/d\alpha$  ( $Ma = 0.5$ ,  $Re = 1500$ , and  $\alpha = 10^\circ$ ).

unsteady adjoint equations were solved at a  $10^\circ$  angle of attack using a fourth-order ESDIRK time integration scheme. As opposed to using the initial condition near the stationary point, the solution at  $t = 100$  was chosen (eliminating the initial transient in the primal, leaving an equilibrium oscillation). Then the flow was integrated over approximately 94 cycles starting from this condition to  $t = 200$ . Finally, the adjoint was integrated backward in time. The convergence history of the time-accurate lift and sensitivity integrand are shown in Fig. 18, along with the running sensitivity integral:

$$\frac{1}{t_f - t} \int_t^{t_f} S(t) dt$$

where  $S(t)$  is the integrand of Eq. (26) at time  $t$ , and the finite difference results from the flow solution. The stationary-point results are also shown for comparison. It was found that the adjoint-based sensitivity is  $3.3737 \text{ rad}^{-1}$  and is plotted as the slope at  $10^\circ$  in Fig. 17. To verify the sensitivity results, a solution was started with the same initial condition at a perturbed angle of attack,  $\pm 0.01^\circ$ , and the results

were finite differenced using central differencing to give an approximate sensitivity of  $3.3742 \text{ rad}^{-1}$  (less than 0.02% different). Note the transient unsteady behavior in the adjoint near  $t = 200$  due to the terminal condition ( $t = 200$ ) of the adjoint variable due to the fixed initial condition ( $t = 100$ ) of the primal. Since the asymptotic behavior of the primal problem is periodic, the sensitivity of the time-average output could be estimated by integrating the sensitivity integrand over a known number of periods. This approach would save computational expense when a periodic behavior can be identified. For a case in which the solution behavior is less ordered, the simulation would have to be run long enough to remove the effects of the primal initial and adjoint terminal conditions.

## VI. Conclusions

The effects of small-scale unsteadiness on adjoint-based output sensitivities were investigated through the use of a viscous subsonic airfoil model problem. This investigation demonstrated the potential for large variability in the estimated output sensitivity using a steady

sensitivity analysis when the nonlinear flow fails to converge to a steady state. Results also showed that iterative methods commonly employed are strong enough to converge to a stationary-point solution, even when there is strong unsteady behavior in the time-accurate solution. An implication of this study is the need to consider unsteady (time-accurate) flow and adjoint analysis even when steady-state solutions can be achieved using strong solvers. Finally, it was shown that the unsteady adjoint provides accurate sensitivities for the time-averaged lift. Future work will focus on applying temporal and spatial adaptation based on an unsteady output error estimate to the small-scale unsteadiness problem, allowing for a smooth transition from solving steady problems to time-accurate unsteady problems.

**Appendix A: Grid and Time-Step Refinement Study**

To verify the accuracy of the time-accurate calculations, the impact of grid and time-step refinement was studied. The dependence of the solution on the time step was considered at 5, 6, 9, and 10° angles of attack using the baseline grid with  $\Delta t = 0.01, 0.1, 0.3,$  and 1.0. Figure A1a plots the difference between the mean lift coefficient

of the three coarser time steps and the mean lift coefficient at the finest time step. The solutions with  $\Delta t = 0.01$  are sufficiently more accurate than the other time steps, such that the difference is a good approximation of the temporal error. For the four angles of attack, the difference decreases by approximately four orders of magnitude for a time-step change from 1.0 to 0.1, implying that the time stepping is in the asymptotic fourth-order-accurate range. The temporal error in the mean lift coefficient with  $\Delta t = 0.1$  is less than  $10^{-4}$  for all of the angles of attack and less than  $10^{-6}$  for the  $\alpha = 10^\circ$  case. Figure A1b shows the time-accurate evolution of the solution at 10° for several time steps. The coarse time step varies significantly from the fine time-step solution, while the medium time step shows good agreement. The medium time step ( $\Delta t = 0.1$ ) was used elsewhere in this study.

A single uniform grid refinement is shown for  $\alpha = 5, 6, 9,$  and 10° in Fig. A2. For 5°, there is a difference in the unsteadiness between the baseline and refined grids, but it remains relatively small. At 6°, the degree of unsteadiness is similar, with an apparent shift in time. At larger angles of attack, however, the differences diminish. While further grid refinement studies could be conducted, we believe the flow does become unstable somewhere below 6°.

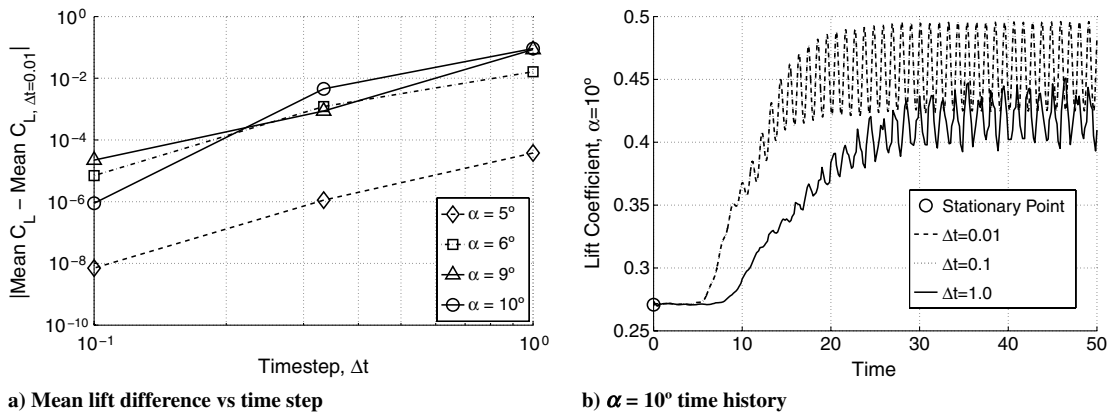


**Fig. A1 Time-step study for unsteady NACA 0012 at  $Ma = 0.5$  and  $Re = 1500$ .**

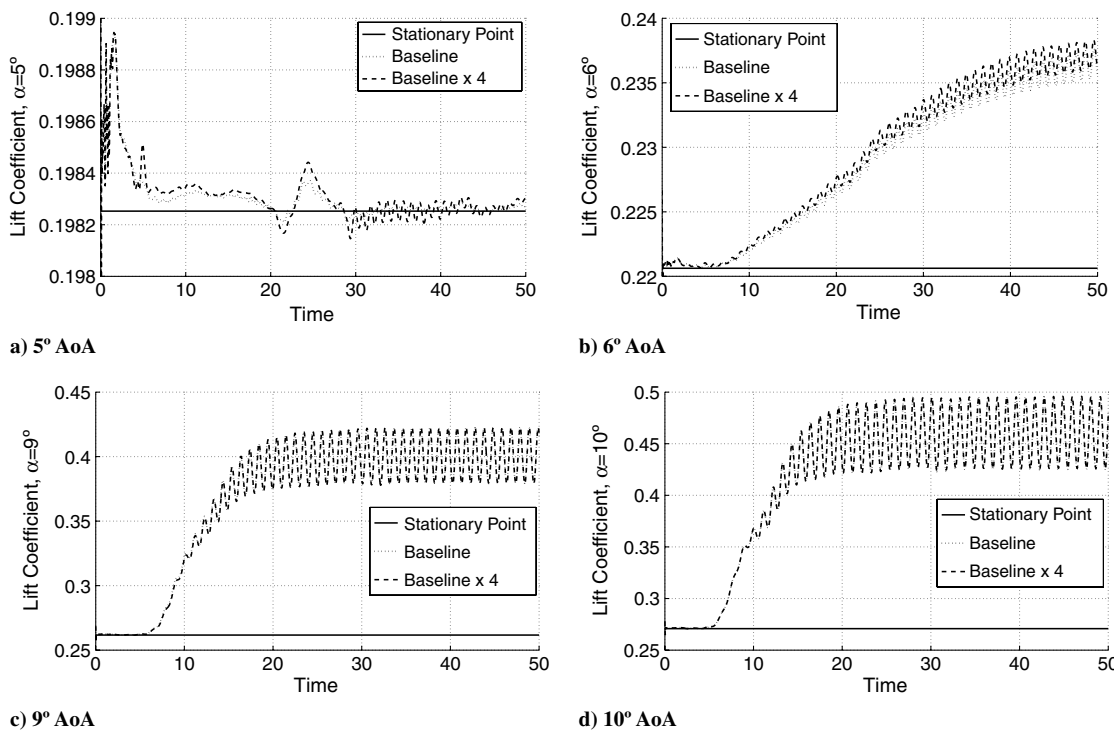


**Fig. A2 Grid study for unsteady NACA 0012 at  $Ma = 0.5, Re = 1500,$  and  $\Delta t = 0.01$  with ESDIRK4.**

## Acknowledgments

The authors would like to acknowledge preliminary work done by Eric Liu and Eleanor Lin. This work was partially funded by The Boeing Company Learning Together Program.

## References

- [1] Bryson, A. E., and Ho, Y. C., *Applied Optimal Control*, Blaisdell, London, 1969.
- [2] Hall, M. C. G., "Application of Adjoint Sensitivity to an Atmospheric General Circulation Model," *Journal of the Atmospheric Sciences*, Vol. 43, No. 22, 1986, pp. 2644–2652. doi:10.1175/1520-0469(1986)043<2644:AOASTT>2.0.CO;2
- [3] Talagrand, O., and Courtier, P., "Variational Assimilation of Meteorological Observations with the Adjoint Vorticity Equation. I: Theory," *Quarterly Journal of the Royal Meteorological Society*, Vol. 113, 1987, pp. 1311–1328. doi:10.1256/smsj.47811
- [4] Derber, J. C., "A Variational Continuous Assimilation Technique," *Monthly Weather Review*, Vol. 117, No. 11, 1989, pp. 2437–2446. doi:10.1175/1520-0493(1989)117<2437:AVCAT>2.0.CO;2
- [5] Jameson, A., "Aerodynamic Design via Control Theory," *Journal of Scientific Computing*, Vol. 3, 1988, pp. 233–260. doi:10.1007/BF01061285
- [6] Giles, M. B., and Pierce, N. A., "An Introduction to the Adjoint Approach to Design," *Flow, Turbulence and Combustion*, Vol. 65, 2000, pp. 393–415. doi:10.1023/A:1011430410075
- [7] Nielsen, E. J., and Anderson, W. K., "Recent Improvements in Aerodynamic Design Optimization on Unstructured Meshes," *AIAA Journal*, Vol. 40, No. 6, 2002, pp. 1155–1163. doi:10.2514/2.1765
- [8] Pierce, N. A., and Giles, M. B., "Adjoint Recovery of Superconvergent Functionals from PDE Approximations," *SIAM Review*, Vol. 42, No. 2, 2000, pp. 247–264. doi:10.1137/S0036144598349423
- [9] Becker, R., and Rannacher, R., "An Optimal Control Approach to a Posteriori Error Estimation in Finite Element Methods," *Acta Numerica*, Vol. 10, 2001, pp. 1–102. doi:10.1017/S0962492901000010
- [10] Barth, T. J., and Larson, M. G., "A Posteriori Error Estimates for Higher Order Godunov Finite Volume Methods on Unstructured Meshes," *Finite Volumes for Complex Applications III*, edited by R. Herban, and D. Kröner, Hermes Penton, London, 2002.
- [11] Giles, M. B., and Süli, E., "Adjoint Methods for PDEs: A Posteriori Error Analysis and Postprocessing by Duality," *Acta Numerica*, Vol. 11, 2002, pp. 145–236. doi:10.1017/CBO9780511550140.003
- [12] Hartmann, R., and Houston, P., "Error Estimation and Adaptive Mesh Refinement for Aerodynamic Flows," *36th CFD/ADIGMA Course on HP-Adaptive and HP-Multigrid Methods*, VKI Lecture Series 2010-01, edited by H. Deconinck, Von Karman Institute for Fluid Dynamics, Rhode-St-Genèse, Belgium, 2009.
- [13] Fidkowski, K., and Darmofal, D., "Output Error Estimation and Adaptation in Computational Fluid Dynamics: Overview and Recent Results," AIAA Paper 2009-1303, 2009.
- [14] Oliver, T., and Darmofal, D., "An Unsteady Adaptation Algorithm for Discontinuous Galerkin Discretizations of the RANS Equations," AIAA Paper 2007-3940, 2007.
- [15] Campobasso, M. S., and Giles, M. B., "Effects of Flow Instabilities on the Linear Analysis of Turbomachinery Aeroelasticity," *Journal of Propulsion and Power*, Vol. 19, No. 2, 2003, pp. 250–259. doi:10.2514/2.6106
- [16] Giles, M. B., "On the Iterative Solution of Adjoint Equations," *Automatic Differentiation: From Simulation to Optimization*, edited by G. Corliss, C. Faure, A. Griewank, L. Hascoet, and U. Naumann, Springer, New York, 2001.
- [17] Nemeč, M., Aftosmis, M. J., and Wintzer, M., "Adjoint-Based Adaptive Mesh Refinement for Complex Geometries," AIAA Paper 2008-725, 2008.
- [18] Saad, Y., and Schultz, M. H., "GMRES: A Generalized Minimal Residual Algorithm for Solving Nonsymmetric Linear Systems," *SIAM Journal on Scientific and Statistical Computing*, Vol. 7, No. 3, 1986, pp. 856–869. doi:10.1137/0907058
- [19] Shroff, G. M., and Keller, H. B., "Stabilization of Unstable Procedures: The Recursive Projection Method," *SIAM Journal on Numerical Analysis*, Vol. 30, No. 4, 1993, pp. 1099–1120. doi:10.1137/0730057
- [20] Campobasso, M. S., and Giles, M. B., "Stabilization of a Linear Flow Solver for Turbomachinery Aeroelasticity Using Recursive Projection Method," *AIAA Journal*, Vol. 42, No. 9, 2004, pp. 1765–1774. doi:10.2514/1.1225
- [21] Griewank, A., and Walther, A., "Revolve: An Implementation of Checkpointing for the Reverse or Adjoint Mode of Computational Differentiation," *ACM Transactions on Mathematical Software*, Vol. 26, No. 1, 2000, pp. 19–45. doi:10.1145/347837.347846
- [22] Nadarajah, S. K., and Jameson, A., "Optimal Control of Unsteady Flows Using a Time Accurate Method," AIAA Paper 2002-5436, 2002.
- [23] Mani, K., and Mavriplis, D. J., "An Unsteady Discrete Adjoint Formulation for Two-Dimensional Flow Problems with Deforming Meshes," AIAA Paper 2007-60, 2007.
- [24] Mavriplis, D. J., "Solution of the Unsteady Discrete Adjoint for Three-Dimensional Problems on Dynamically Deforming Unstructured Meshes," AIAA Paper 2008-727, 2008.
- [25] Rumpfkeil, M. P., and Zingg, D. W., "Unsteady Optimization Using a Discrete Adjoint Approach Applied to Aeroacoustic Shape Design," AIAA Paper 2008-18, 2008.
- [26] Roe, P. L., "Approximate Riemann Solvers, Parameter Vectors, and Difference Schemes," *Journal of Computational Physics*, Vol. 43, No. 2, 1981, pp. 357–372. doi:10.1016/0021-9991(81)90128-5
- [27] Bassi, F., and Rebay, S., "GMRES Discontinuous Galerkin Solution of the Compressible Navier–Stokes Equations," *Discontinuous Galerkin Methods: Theory, Computation and Applications*, edited by K. Cockburn, and Shu, Springer, Berlin, 2000, pp. 197–208.
- [28] Wang, L., and Mavriplis, D. J., "Implicit Solution of the Unsteady Euler Equations for High-Order Accurate Discontinuous Galerkin Discretizations," AIAA Paper 2006-0109, 2006.
- [29] Diosady, L. T., and Darmofal, D. L., "Preconditioning Methods for Discontinuous Galerkin Solutions of the Navier–Stokes Equations," *Journal of Computational Physics*, Vol. 228, 2009, pp. 3917–3935. doi:10.1016/j.jcp.2009.02.035

T. Zang  
Associate Editor